ADVANCED PHOTONICS RESEARCH
Open Access
www.adpr-journal.com

Downshifting Layer of Europium-Doped $NaGdF_4$: From the Optimization of the Sol–Gel Process to the Luminescent Properties

Anna Lucia Pellegrino, Francesca Lo Presti, Francesca Loschi, Adolfo Speghini, and Graziella Malandrino**

The key issue for a wide application of solar energy is the possibility to establish an innovative photovoltaic technology that allows a more efficient energy conversion. In this direction, the use of additional layers in the well-established silicon-based modules represents a challenging strategy. In this context, the present work is devoted to the optimization of a downshifting (DS) system made of the $NaGdF_4$ matrix in the form of thin film as a host material for the europium-luminescent ions. The Eu-doped $NaGdF_4$ system is fabricated through a sol–gel approach starting from a mixture of Na(hfa)•tetraglyme, $Gd(hfa)_3$•diglyme, and $Eu(hfa)_3$•diglyme in ethanol solution. The operative parameters are finely tuned to pursue the formation of compact and polycrystalline films. Particularly, the annealing treatment, the nature of the substrate, and the doping ion percentage are the key parameters for the reproducible and selective formation of $NaGdF_4$ in the form of the beta (hexagonal) crystal structure with promising luminescent properties. Morphological, structural, and compositional features are deeply studied through field-emission scanning electron microscopy, X-ray diffraction analysis, and energy-dispersive X-ray analysis, respectively. The luminescence investigations confirm the properties of the Eu-doped $NaGdF_4$ as DS system.

1. Introduction

In the last decades, sodium rare-earth (RE) tetrafluorides $NaREF_4$, with Y, Gd, La, or Lu as RE, have been deeply investigated as inorganic hosts for energy conversion (EC) systems doped with luminescent Ln^{3+} ions.[1–3] $NaREF_4$ materials, indeed, are considered to be one of the most efficient host classes for EC systems, providing highly efficient luminescence emissions due to their lower lattice phonon energy and their high chemical stability.[4–7] The most studied Ln^{3+} activators are Yb^{3+} and Er^{3+}, Pr^{3+} or Tm^{3+} for upconverting systems, and Eu^{3+} for downshifting (DS) systems.[8–10]

The EC processes can be achieved through two main processes: 1) upconversion (UC), in which photons with energies in the near-infrared region are converted into higher energy photons, typically in the visible or ultraviolet (UV) range; and 2) down-conversion (DC) and DS processes, based on the principle of Stokes shift, where high energy photons are converted into lower energy radiations.

These systems have attracted much attention due to their wide use for several photonic applications, such as infrared and tunable phosphors, sensing, solar cells, and bioimaging.[11–14]

Interestingly, among several technological applications, the insertion of luminescence material in a solar cell device represents a good strategy to extend the solar response to both the near infrared and the UV regions, which can further increase the device efficiency. Recently, J. Wu et al. have reported a study in which by adding $NaGdF_4:Er^{3+}/Yb^{3+}$ nanorods into chlorobenzene antisolvent during the preparation of the perovskite active layer, they found that UC luminescence nanoparticles could effectively improve the perovskite solar cell performance.[3,15] Other type of europium-doped materials based on phosphates and molybdates are interesting for light emitting diode[16] and anti-counterfeiting[17] applications.

For this application, the possibility of having doped $NaGdF_4$ fluoride in the form of thin films is highly desirable in order to reach a homogeneous coverage and an enhancement of the luminescence properties. To the best of our knowledge, only one work is reported in the literature on the fabrication of UC $NaGdF_4$ as massive thin films using electrodeposition method by H. Jia and co-workers,[18] while no studies are known on DS or DC $NaGdF_4$-based films.

A. L. Pellegrino, F. Lo Presti, G. Malandrino
Dipartimento di Scienze Chimiche
Università di Catania and INSTM UdR Catania
V.le A. Doria 6, 95125 Catania, Italy
E-mail: annalucia.pellegrino@unict.it; graziella.malandrino@unict.it

F. Loschi, A. Speghini
Nanomaterials Research Group (NRG) - Dipartimento di Biotecnologie
Università di Verona and INSTM UdR Verona
Strada le Grazie 15, 37134 Verona, Italy

The ORCID identification number(s) for the author(s) of this article can be found under https://doi.org/10.1002/adpr.202400153.

DOI: 10.1002/adpr.202400153

In this field of application, thus, the possibility to design $NaGdF_4$-based materials in the form of thin film, with a tuning of both structural and compositional features represents a bottleneck. Currently, the most common synthetic procedures for $NaGdF_4$-based materials include thermal decomposition, coprecipitation, and solvothermal methods.[19–22] The sol–gel approach has been tested as well for the growth of $NaGdF_4$ in the form of nanoparticles or composites.[23] In this direction, great effort has been devoted to the formation of thin films as transparent oxyfluoride nano-glass–ceramics containing Ln-doped $NaREF_4$ in the form of nanocrystals or nanoparticles. Velázquez et al. reported the synthesis of transparent oxyfluoride nano-glass–ceramics containing undoped and 0.5 Eu^{3+}-doped $NaGdF_4$ nanocrystals.[24]

Notably, the $NaGdF_4$ phase exists in two polymorphic forms: cubic (α) and hexagonal (β), with the latter phase being the most efficient host matrix for EC processes, thus playing a pivotal aspect in the engineering of the final functional materials.[25] Thus, to achieve the optimal EC properties, a fine engineering of the nanostructure features, i.e. in thin film forms for photovoltaic (PV) application, and the good homogeneity of the luminescence centers are highly desirable.

In the present work, we report for the first time the optimization of the sol–gel/spin-coating approach for the synthesis of down-converting layer of Eu-doped $NaGdF_4$ film starting from a solution of Na(hfa)•tetraglyme, $Gd(hfa)_3$•diglyme, and $Eu(hfa)_3$•diglyme precursors. A fine tailoring of the annealing process has been the key point for the stabilization of the $NaGdF_4$ as cubic and/or hexagonal crystalline structure in a reproducible and selective way. The effect of the process parameter has been investigated also on the morphological features of the undoped and Eu-doped films. To our knowledge, this work represents the first report on synthesizing compact Eu-doped $NaGdF_4$ systems through a sol–gel approach. The crystalline structure and the morphological and compositional features of the as-prepared $NaGdF_4$ thin film have been in-depth studied through X-ray diffraction analysis (XRD), field-emission scanning electron microscopy (FE-SEM), and energy-dispersive X-ray analysis (EDX), respectively. The functional properties of the Eu-doped films as DS layer have been investigated through luminescence measurements under UV irradiation.

2. Results and Discussion

For the sake of clarity, a scheme of a combined sol–gel/spin-coating process and the annealing treatments tested in the present work is shown in **Figure 1**. Na(hfa)•tetraglyme, $Gd(hfa)_3$•diglyme, and $Eu(hfa)_3$•(diglyme) have been successfully applied for the sol–gel synthesis of undoped and Eu-doped $NaGdF_4$ phase. The deposition process of the sol has been conducted through a spin-coating procedure in order to obtain the desired material as thin films. A multistep procedure in which the spin-coating process is alternated with a fast-annealing treatment ensures the formation of compact layers, as already established in our previous work for Ln-doped CaF_2 and $NaYF_4$ films.[26–28]

Structural characterization of the undoped and doped systems has been performed through XRD analysis and reported in **Figure 2** as a function of the annealing temperatures, doping percentage and substrate nature. The effect of the annealing treatment in the phase formation and in the stabilization of the hexagonal $NaGdF_4$ structure has been observed in the patterns reported in Figure 2a. In particular, at lower annealing temperatures, i.e., 200 °C, the diffractogram displays only barely visible peaks at 27.6°, 45.9°, and 54.4°, which could be likely assigned to the 111, 220, and 311 reflections of the cubic phase. At the temperature of 250 °C, the pattern shows several peaks associated with the formation of the pure β-$NaGdF_4$ phase film. The stabilization of the hexagonal phase under this condition is also confirmed at higher annealing temperatures, i.e., 300, 350, and 400 °C, with an increase in the peak intensities, suggesting the formation of a highly crystalline β-$NaGdF_4$ structure. Notably, the selective stabilization of the pure β-$NaGdF_4$, using an annealing temperature as low as 250 °C, represents an added value of the current synthetic approach, due to the very low thermal budget required. The effect of the Eu doping ions in the structure has been investigated as well. Both the undoped and 10% Eu-doped $NaGdF_4$ samples show the formation of the pure hexagonal structure without any impurities (Figure 2b). Considering the similar ionic radii of the Eu^{3+} and Gd^{3+}, 1.12 and 1.107 Å, respectively, located in nine coordinated sites, it is likely that the Eu ions are substitutional to Gd.[29] This trend was recently confirmed in our previous work on the analogous $NaYF_4$ system doped with Yb^{3+} and Tm^{3+} species.[27] Furthermore, the β phase is obtaineds independently on the substrate nature, as shown in Figure 2c, for the 10% Eu-doped $NaGdF_4$ films grown on silicon and quartz substrates. Thus, the treatment temperature plays a key role in determining the $NaGdF_4$ structure, while the substrate does not affect the nature of the formed crystalline structure.

Morphological characterization has been carried out through FE-SEM on samples obtained at different annealing temperatures and reported in **Figure 3**. All the morphologies obtained suggest a good adhesion of the film onto the substrate during the deposition processes and thus confirm the formation of a well-reticulated gel. Particularly, the $NaGdF_4$:10% Eu sample obtained at 200 °C (Figure 3a) shows the formation of a homogeneous film over a large area and a very smooth surface that can be likely due to the formation of the low crystallinity cubic $NaGdF_4$ phase (see Figure 2a, black line). The samples treated at 250 and 300 °C in Figure 3b,c, respectively, display, indeed, a well-structured and porous structures, associable to the more crystalline features of the $NaGdF_4$:10% Eu as β phase. Finally, at higher annealing temperatures, i.e., 350 and 400 °C in Figure 3d, e, the surfaces present slightly more porous structures and the formation of some outgrowths. This evidence can be rationalized considering different aspects: 1) the density of the sol and the good wettability of the substrates are responsible for the homogeneous and compact coverage independently from the subsequent temperature treatment; 2) the features of the films in terms of flat or porous structure are due to the annealing steps. This second trend can be likely due to different solvent evaporation and/or densification at the various intermediate and final annealing temperatures. Furthermore, the atomic force microscopy (AFM) characterization of the β-$NaGdF_4$:10% Eu films at 200, 300, and 400 °C (Figure 3a',c',e') confirms as well the homogeneity of the layers with fully coalesced grains, and the increase of the surface porosity with a root mean square roughness

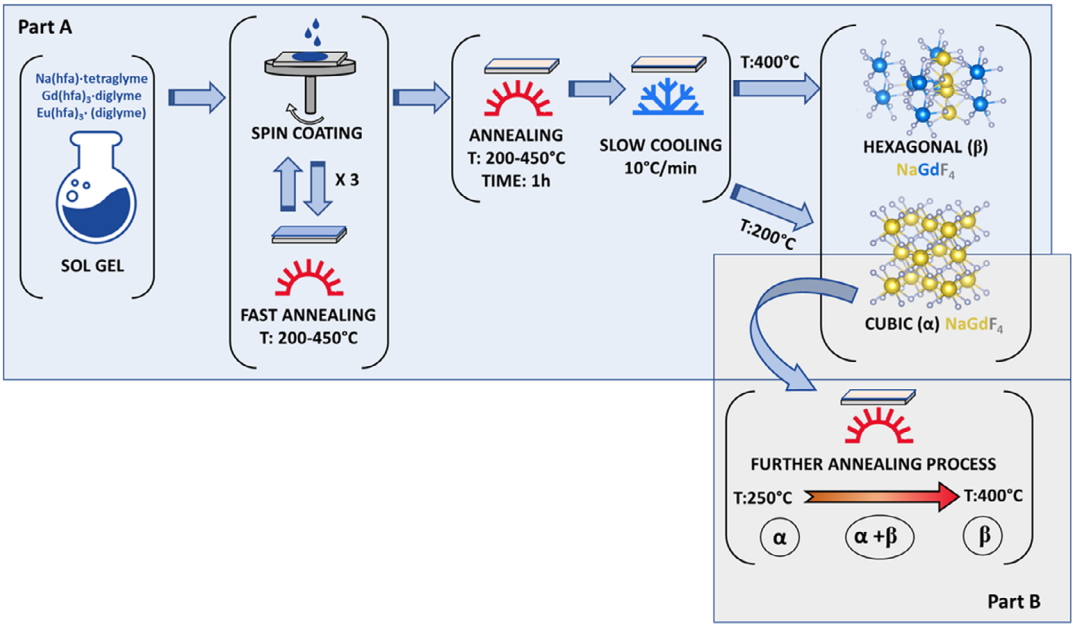

Figure 1. Scheme of the synthetic process from the sol–gel and spin-coating deposition to the annealing treatments of the films: Part A) indicates that films are obtained through a direct temperature treatment at the indicated temperature; Part B) indicates that films are obtained as cubic phase at 200 °C and subsequently treated at increasing temperature. The structures were derived through the Vesta program using the cif of ref. [40] for the hexagonal structure.

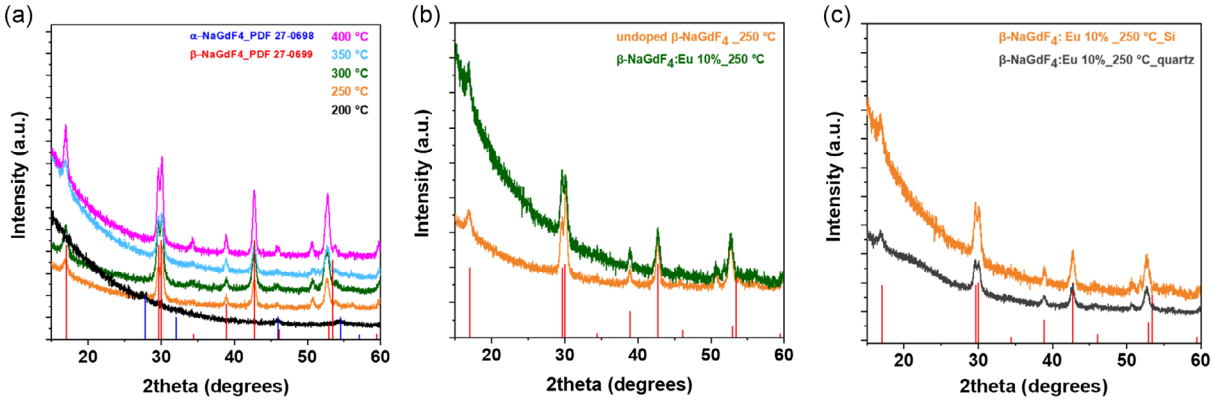

Figure 2. XRD patterns of a) undoped $NaGdF_4$ films on Si (100) as a function of the annealing treatment; b) comparison of undoped and β-$NaGdF_4$: 10% Eu films obtained at 250 °C on Si (100); and c) β-$NaGdF_4$:10% Eu films deposited of Si and quartz substrates.

(measured on a 10 × 10 μm area) of about 29, 53, and 61 nm, respectively.

Thereafter, the effect of post-additional annealing treatment on the sample $NaGdF_4$:10% Eu on Si obtained at 200 °C is illustrated in **Figure 4**. The XRD pattern of the sample $NaGdF_4$:10% Eu treated first at 200 °C displays very weak signals related to the presence of the cubic phase, as already observed for the undoped analog sample (see Figure 2a, black line). This film has been subjected to post-annealing treatment at 250 °C in air for 1 h, confirming the formation of the cubic phase due to the presence of well-defined peaks at 27.86°, 32.10°, 46.06°, and 54.60°, associated with the 111, 200, 220, and 311 planes of the cubic structure. After that, under the same operative conditions, the sample has been treated at the temperature of 300 and 350 °C. The patterns obtained in this case match the formation of both cubic and hexagonal $NaGdF_4$ phases, as confirmed by the presence of additional peaks at 16.95°, 29.63°, 30.10°, 38.85°, 42.66°, and 52.65° due to the β phase. Finally, another annealing treatment at 400 °C has been executed resulting in the stabilization of the pure hexagonal phase, without the presence of any peaks associable to the cubic one.

This interesting trend can be rationalized by considering a different balance between kinetic and thermodynamic aspects in the stabilization of the β versus α phase. In the case of samples directly annealed at the final temperatures from 200 to 400 °C (see Figure 2), a low-crystalline cubic phase is observed at the

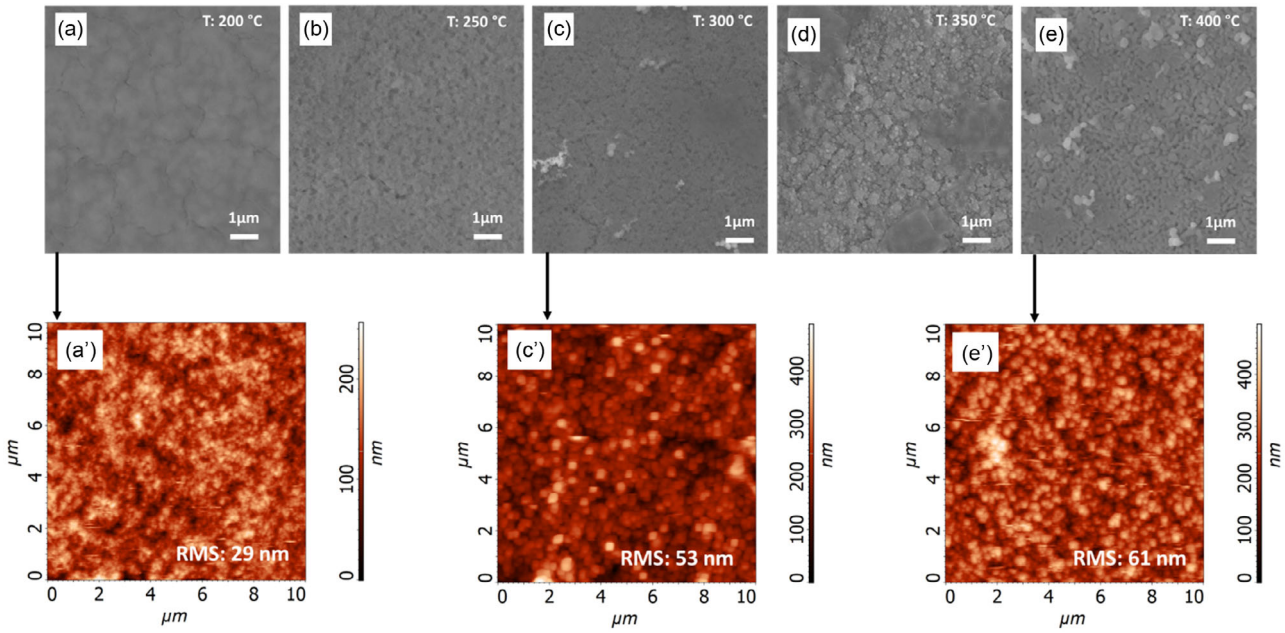

Figure 3. FE-SEM images of the β-$NaGdF_4$:10% Eu films deposited onto Si (100) substrate with annealing treatment at a) 200 °C; b) 250 °C; c) 300 °C; d) 350 °C; and e) 400 °C. The corresponding AFM topographical images of β-$NaGdF_4$:10% Eu films at a') 200 °C; c') 300 °C; and e') 400 °C are shown.

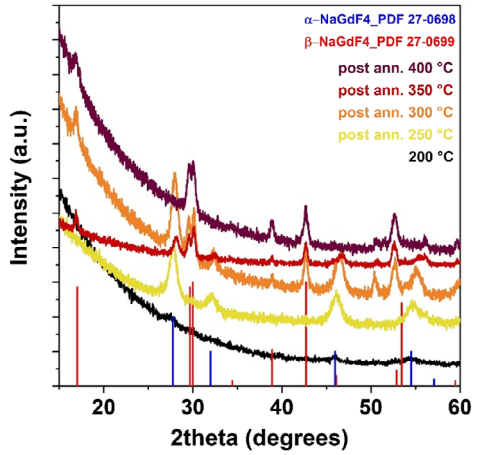

Figure 4. XRD patterns of the $NaGdF_4$:10% Eu film on Si (100) initially annealed at 200 °C and sequentially treated at temperatures of 250, 300, 350, and 400 °C for 1 h.

lowest temperature (200 °C), while the pure hexagonal phase stabilizes already at 250 °C, suggesting that the β phase is more thermodynamically stable. Conversely, the sequential annealing treatments of the same sample (Figure 4), in which the 200 °C produced low-crystalline cubic phase is sequentially subjected to a heating process of 1 h at T: 250, 300, 350, and 400 °C, seems to favor the stabilization of the cubic phase at the lowest temperatures (250–350 °C), and the hexagonal one at higher temperatures. This result suggests that the formation of the cubic phase grains at 200 °C may act as seeds for the stabilization of the pure, crystalline α phase at 250 °C.

The morphological characterization associated with the sequential annealing treatments commented earlier is shown in **Figure 5**. The $NaGdF_4$:10% Eu film treated at 250 °C in Figure 5a displays a homogeneous, compact, and flat surface which is quite similar to the one found for the $NaGdF_4$:10% Eu sample obtained at 200 °C (Figure 3a).

In addition, only a few outgrowths are barely visible. The morphology remains almost unchanged during the treatment at 300 and 350 °C (see Figure 5b,c). Finally, the film treated at 400 °C in Figure 5d shows a comparable flat surface.

The compositional features of the $NaGdF_4$ films have been assessed through EDX analysis to ensure both the clean fabrication process and the well-controlled amount of Eu doping ions for DS properties. In **Figure 6**, the spectra of the 10% and 15% Eu-doped β-$NaGdF_4$ films, obtained on Si (100) at 350 °C, have been reported. Notably, all the samples show the peaks at 0.67 and 1.06 keV due to the K_α peaks of fluorine and sodium, respectively, together with the signals at 1.20 keV, and in the range of 6.04–7.3 keV arising from the M_α and L lines, respectively, of the gadolinium. The spectra display also the peaks due to the L lines of the europium in the range of 5.60–6.8 keV. Notably, the absence of peaks associable to the presence of C in all the spectra points to an efficient sol–gel process of the precursors, which do not remain as unreacted impurities. The peaks of O and Si at 0.54 and 1.74 keV, respectively, are instead arising from the substrate. Interestingly, the quantitative analyses reported in the table in Figure 6 confirm the correct stoichiometry of the $NaGdF_4$ phase, with a Na:Gd ratio of about 1:0.95, and the Eu percentages of 8.5% and 13.1% for the β-$NaGdF_4$:10% Eu and 15% Eu films, respectively, which match the values set in the starting mixtures.

2.1. Luminescence Characterization

The Eu-doped $NaGdF_4$ samples, used for the luminescence characterization, have been prepared following the procedure

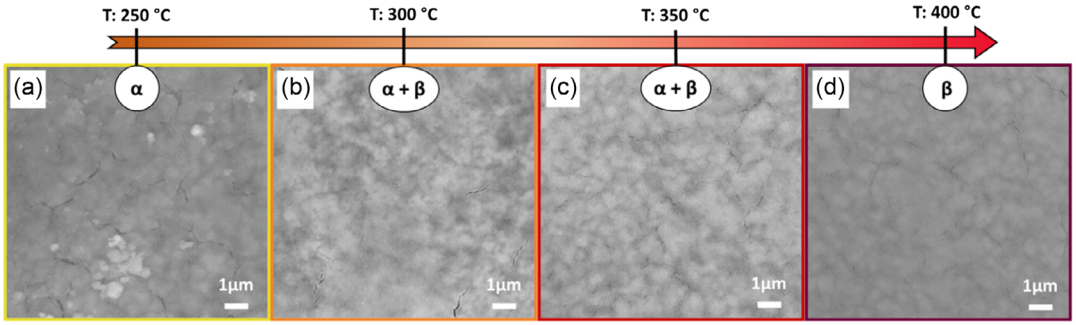

Figure 5. FE-SEM images of a $NaGdF_4$:10% Eu film on Si (100) sequentially treated in temperature at a) 250 °C, b) 300 °C, c) 350 °C, and d) 400 °C for 1 h.

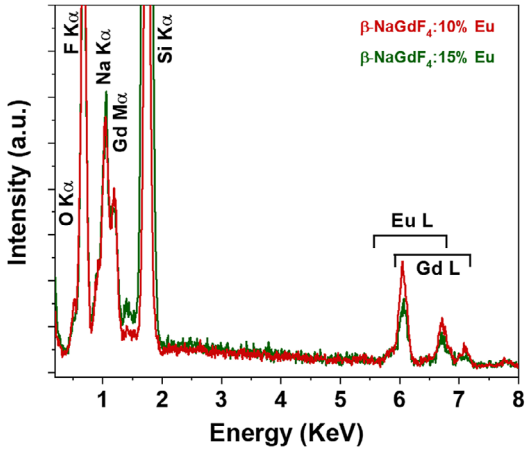

	β-$NaGdF_4$: 10% Eu	β-$NaGdF_4$: 15% Eu
ELEMENT	Atomic %	
F (K)	47.24	56.64
Na (K)	12.13	15.43
Eu (L)	1.03	1.86
Gd (L)	11.12	12.31

Figure 6. EDX spectra of the β-$NaGdF_4$:10% Eu and 15% Eu films obtained at 350 °C on Si (100) and related table with atomic percentages.

described in Figure 1, Part A. The excitation spectra of the lanthanide-doped $NaGdF_4$ film samples show a series of bands typical of the Eu^{3+} ions, as shown in **Figure 7**. In particular, the strongest band around 395 nm is due to the $^7F_0 \rightarrow {}^5L_6$ transition. Other bands are observed due to other transitions, mainly from the $^7F_0$ (ground state). Furthermore, the first excited level, $^7F_1$, is populated at room temperature according to the Boltzmann distribution law:

$$\frac{N_1}{N_0} = e^{-\frac{\Delta E}{k_B T}} \quad (1)$$

where N_1 and N_0 represent the $^7F_1$ and the $^7F_0$ ground-state populations, respectively, k_B is the Boltzmann constant, T is the absolute temperature, and ΔE is the energy gap between the two coupled levels.[30]

A transition starting from the populated $^7F_1$ level gives rise to the excitation band located around 535 nm (see Figure 7).

Room-temperature emission spectra of the Eu^{3+}-doped $NaGdF_4$ films, deposited on Si (100) and on quartz substrates at several annealing temperatures, are shown in **Figure 8**. All the samples exhibit emission bands due to transitions of the Eu^{3+} ions from the $^5D_0$ excited level to the lower-lying ^7F_J multiplets ($J = 0, 1, 2, 3, 4$). The two main observed bands in all the spectra correspond to the $^5D_0 \rightarrow {}^7F_1$ (in the 580–600 nm range) and $^5D_0 \rightarrow {}^7F_2$ transitions (in the 605–630 nm). While the $^5D_0 \rightarrow {}^7F_2$ transition is electric dipole allowed, only for lanthanide sites

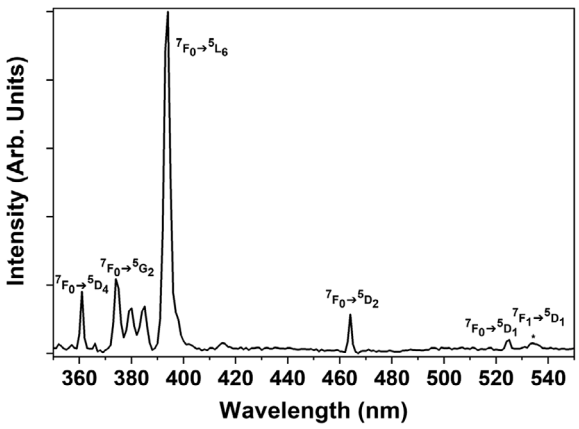

Figure 7. Excitation spectrum ($\lambda_{em} = 615$ nm) for the β-$NaGdF_4$:10% Eu film on Si (100) prepared at 350 °C (Figure 1, Part A) and band assignments.

without inversion symmetry, the $^5D_0 \rightarrow {}^7F_1$ transition is a magnetic dipole transition, not dependent on the local environment around the lanthanide ion.[31] The ratio between the intensities of the emission bands due to these two transitions is useful for investigating the asymmetry of the local environment of the Eu^{3+} ions.[32] The important quantity called asymmetry ratio (R) is defined as

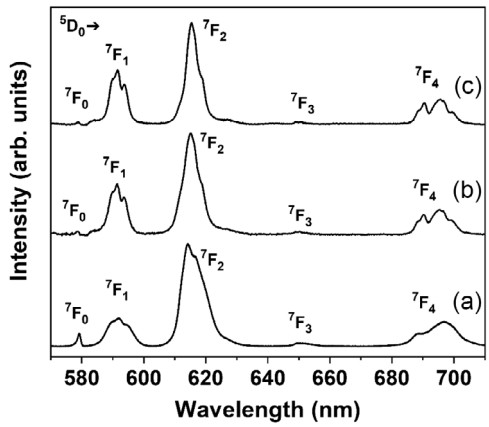

Figure 8. Emission spectra ($\lambda_{exc} = 390$ nm) for a) film of $NaGdF_4$:10% Eu on quartz, prepared at 200 °C; b) film of β-$NaGdF_4$:10% Eu on Si (100), prepared at 350 °C; and c) film of β-$NaGdF_4$:15% Eu on Si (100), prepared at 350 °C. All these samples have been prepared following the procedure described in Figure 1, Part A.

$$R = A(^5D_0 \rightarrow {}^7F_2)/A(^5D_0 \rightarrow {}^7F_1) \quad (2)$$

where A represents the integrated area of the $^5D_0 \rightarrow {}^7F_J$ ($J = 1, 2$) transitions. R is highly dependent on the symmetry of the site where the lanthanide ion is accommodated: the R value increases on decreasing the degree of the lanthanide site symmetry. The $NaGdF_4$ film prepared at 200 °C on quartz shows emission bands typical of Eu^{3+} ions in a very disordered environment. The calculated R value for this sample is 3.9 ± 0.2, denoting a remarkable asymmetry of the site (Figure 8a). This observation is compatible with the presence of a predominant amorphous structure for the sample, demonstrated by its XRD pattern (Figure 4), in which very low intensity reflections for the α-$NaGdF_4$ phase are observed.

Differently, the emission spectrum for the β-$NaGdF_4$:10% Eu film prepared at 350 °C (Figure 8b) is compatible with that observed for Eu^{3+}-doped β-$NaGdF_4$ nanocrystals by Ptacek et al. prepared by a wet chemical synthesis.[33,34] Moreover, the observed emission spectrum is also in agreement with that found by Ghosh et al. for hexagonal nanorods prepared by a solvothermal method involving an ionic liquid technique.[35] For this sample, the asymmetry R value is 2.5 ± 0.1, indicating a higher symmetric environment around the lanthanide ion with respect to the mainly amorphous $NaGdF_4$:10% sample prepared at 200 °C. Similarly, the emission spectrum of the β-$NaGdF_4$:15% Eu sample prepared at 350 °C (Figure 8c) is also typical of Eu^{3+}-doped β-$NaGdF_4$, in agreement with the XRD results (Figure 4). For this thin film, the calculated R value is 1.9 ± 0.1, confirming the slight asymmetry around the lanthanide ion, similar to what has been found in the previous sample. The slight difference between the R values for the two differently doped β-$NaGdF_4$ samples prepared at 350 °C indicates a different local environment around the Eu^{3+} ion. In particular, the 15% doped sample is characterized by a slightly more symmetric environment for the Eu^{3+} ions with respect to the 10% doped sample.

To get further insight into the dynamics of the lanthanide excited states, we measured the emission decay curves for the β-$NaGdF_4$:10% and 15% Eu-doped films on Si (100) prepared at 350 °C and the $NaGdF_4$:10% film on Si (100) prepared at 200 °C. To this aim, we monitored the emission at 615 nm, corresponding to the $^5D_0 \rightarrow {}^7F_2$ transition, and the decay curves are shown in **Figure 9**.

The emission curves for the β-$NaGdF_4$ samples show a strong non-exponential behavior, suggesting different local environments for the Eu^{3+} ions. The emission intensity I of the decay curves (shown in Figure 9) has been fitted with a biexponential function, defined as

$$I = \sum_i A_i \exp\left(-\frac{t}{\tau_i}\right) \quad (3)$$

where A_i and t_i represent the weight and decay time of the ith contribution. The intensity-weighted average lifetimes t_{av} are defined as[36]

$$\tau_{av} = \frac{\sum_i A_i \tau_i^2}{\sum_i A_i \tau_i} \quad (4)$$

The calculated values of weights, decay times, and intensity-weighted average lifetimes are reported in **Table 1**.

Remarkably, the intensity-weighted lifetime of the $^5D_0$-excited energy level results is 3.86 ± 0.06 ms for the β-$NaGdF_4$:10% Eu on Si (100), prepared at 350 °C. This value is similar to that found by Van Do et al. (4.72 ms)[37] for nanocrystalline $NaGdF_4$ doped with 10% of Eu^{3+} ions, a value much smaller than for lighter-doped $NaGdF_4$ samples. In the present sample, since the amount

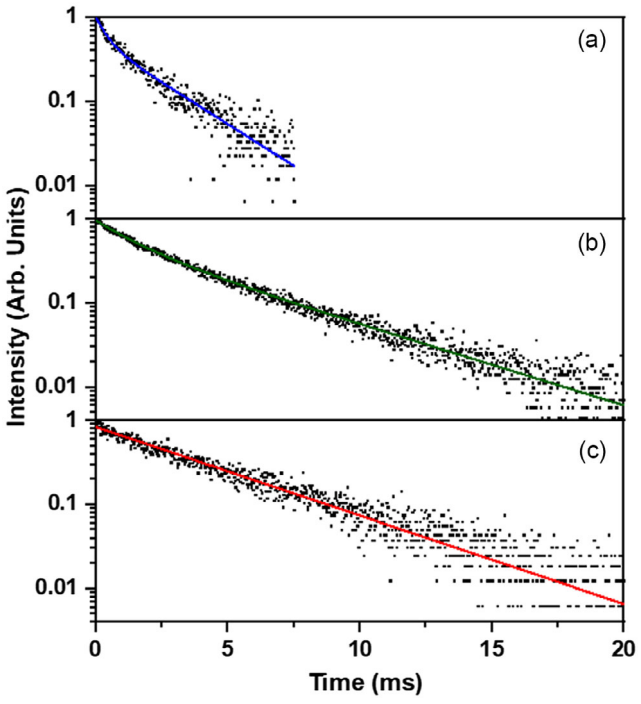

Figure 9. Emission decays ($\lambda_{exc} = 395$ nm, $\lambda_{em} = 612$ nm, $^5D_0 \rightarrow {}^7F_2$ transition) for a) the β-$NaGdF_4$:15% Eu film on Si(100) prepared at 350 °C, b) the β-$NaGdF_4$:10% Eu film on Si(100) prepared at 350 °C, and c) $NaGdF_4$:10% film on Si(100) prepared at 200 °C. Solid lines: exponential fits of the emission decay data.

Table 1. Decay times τ_i ($i = 1, 2$), weights A_i ($i = 1, 2$), and intensity-weighted average lifetimes τ_{avg} calculated by two-exponential fits of the emission decay curves for the β-$NaGdF_4$:10% Eu and 15% Eu films on Si(100) prepared at 350 °C. Decay time calculated by one-exponential fit of the emission decay curve for the $NaGdF_4$:10% Eu film on Si(100) prepared at 200 °C.

Sample	τ_1 [ms]	A_1	τ_2 [ms]	A_2	τ_{avg} [ms]
β-$NaGdF_4$:15% Eu	0.51 ± 0.09	0.55 ± 0.07	2.4 ± 0.1	0.45 ± 0.08	2.1 ± 0.1
β-$NaGdF_4$:10% Eu	1.52 ± 0.05	0.46 ± 0.02	4.57 ± 0.07	0.51 ± 0.02	3.86 ± 0.06
$NaGdF_4$:10% Eu	4.2 ± 0.3				

of Eu^{3+} ion doping is high (10%), the relatively short lifetime of the $^5D_0$ excited energy level is most probably due to energy migration processes among the Eu^{3+} ions. When the excitation energy reaches defect traps, it can be non-radiatively relaxed, therefore diminishing the experimental lifetime. Moreover, the emission decay curve for the β-$NaGdF_4$:15% Eu on Si (100), prepared at 350 °C, is shown in Figure 9a. From the figure, it can be noted that a further increase of the Eu^{3+} concentration in the β-$NaGdF_4$ induces a notable shortening of the lanthanide lifetime, from 3.86 ± 0.06 ms for the 10% doped sample to 2.1 ± 0.1 ms for the 15% doped one. This behavior is perfectly in line with the trend observed by Van Do et al.[37] who found a monotonic decrease of the emission decay times on increasing the Eu^{3+} concentration in nanocrystalline β-$NaGdF_4$.

The emission decay curve for the $NaGdF_4$:10% Eu film on Si (100) prepared at 200 °C is shown in Figure 9c. The experimental data can be reasonably fitted with a single exponential decay, and the result is reported in Table 1. The decay time (4.2 ± 0.3 ms) is similar, within the experimental uncertainties, to that found for the β-$NaGdF_4$ sample with the same Eu^{3+} concentration. Moreover, the decay time is slightly higher than that for a 10% doped sample of α-$NaGdF_4$ nanocrystals (3 ms) found by Ptacek et al.[33]

3. Conclusions

In summary, the present approach proposes a high yield production method, using an inexpensive equipment, for the fabrication of lanthanide-doped ternary fluoride films having high crystallinity and very homogeneous surface. To the best of our knowledge, the herein work is the first report on the fabrication of Eu-doped $NaGdF_4$ thin film using a sol–gel process. Furthermore, the use of Na(hfa)•tetraglyme, $Gd(hfa)_3$•diglyme, and $Eu(hfa)_3$•(diglyme) as starting precursor mixture represents an added value of the process, due to 1) the possibility of easily tune the doping ion percentage and 2) their clean decomposition yielding pure undoped and doped films. In addition, the presence of fluorine, deriving from the fluorinated ligands, makes these compounds single-source precursors for all the required elements, thus avoiding the use of an additional fluorine source.

The annealing treatment and the temperatures tested have reproducibly and selectively allowed to fine control the crystalline structure of the films, i.e., cubic versus hexagonal $NaGdF_4$ structure. Furthermore, the morphological features of the as-prepared systems have been correlated to the annealing temperatures. The incorporation of dopant Eu^{3+} ions in the $NaGdF_4$ films has been established by the luminescence measurements, in particular from emission spectra and decays, which have assessed the energy DS properties of the prepared layers and confirmed the potentiality of the systems as efficient DS layers in PV technology.

4. Experimental Section

Film Preparation: The metalorganic adducts of Na, Gd, and Eu, i.e., Na(hfa)•tetraglyme, $Gd(hfa)_3$•diglyme, and $Eu(hfa)_3$•(diglyme) (where Hhfa = 1,1,1,5,5,5-hexafluoro-2,4-pentanedione), tetraglyme =2,5,8,11, 14-pentaoxapentadecane, and diglyme is bis(2-methoxyethyl) ether), were synthesized as previously reported in refs. [28,38,39].

Starting from a mixture of Na, Gd, and Eu precursors, a water/ethanol solution was prepared for the sol–gel reaction. Under acid condition, established through trifluoroacetic acid, the hydrolysis and condensation reactions took place for a duration of 20 h under stirring and refluxing at 60 °C. The adducts were mixed in different molar ratio values for the preparation of undoped, 10% and 15% of Eu-doped $NaGdF_4$ films, respectively.

The different molar ratios used for the fabrication of the films are reported as in the following: 1) for $NaGdF_4$: 1 Na(hfa)•tetraglyme: 1 $Gd(hfa)_3$•diglyme: 43 C_2H_5OH:1.5 H_2O:0.4 CF_3COOH; 2) for $NaGdF_4$: Eu (10%): 1Na(hfa)•tetraglyme: 0.9 $Gd(hfa)_3$•diglyme: 0.1 $Eu(hfa)_3$• diglyme: 43 C_2H_5OH:1.5 H_2O:0.4 CF_3COOH; and 3) for $NaGdF_4$: Eu(15%): 1Na(hfa)•tetraglyme: 0.85 $Gd(hfa)_3$•diglyme: 0.15 $Eu(hfa)_3$• diglyme: 43 C_2H_5OH:1.5 H_2O:0.4 CF_3COOH.

The deposition process was carried out through spin-coating method on Si (100) and quartz substrates using a multistep procedure in which three times of spin-coating deposition were alternated with fast annealing steps in air for 10 min. Finally, the films were annealed in air for 1 h and a slow cooling step of 10 °C min^{-1} was setup. A wide range of annealing temperatures was tested, from 200 to 400 °C. For the deposition, a Spin-Coater SPIN-150 SPS Europe system was used with a spinning rate of 3000 rpm and a time of 60 s for each step. Different sets of undoped and doped $NaGdF_4$ films were synthesized on Si (100) and quartz at different annealing temperatures. The undoped samples were directly treated at different temperature values, i.e., 200, 250, 300, 350, and 400 °C, for both the intermediate fast annealing and the final annealing step (Figure 1, Part A; and related pattern in Figure 2a). Distinctly, the $NaGdF_4$:10% Eu sample initially annealed at 200 °C was subjected to additional heating treatments at 250, 300, 350, and 400 °C to test the effect of annealing in the already α-$NaGdF_4$-crystallized structure (Figure 1, Part B; Figure 4).

Characterization: Structural characterizations were performed through XRD analysis in grazing incidence mode (0.5°) using a SmartLab Rigaku diffractometer operating at 45 kV and 200 mA, equipped with a rotating anode of Cu K_α radiation. The film morphologies were studied through FE-SEM using a ZEISS SUPRA 55 VP field-emission microscope. Additionally, topographic features of the samples were investigated through AFM adopting an Au-coated silicon probe with a nominal 35 nm tip curvature radius and a typical force constant of 0.1 N. Quantitative analysis of the doped samples was performed through EDX analysis, recorded using an INCA-Oxford windowless detector, having a resolution of 127 eV as the full-width half-maximum of the Mn K_α.

Spectroscopic Characterization: The emission spectra were excited using a UV light-emitting diode (LED) flashlight and a band pass filter centered at 390 nm. The spectra were collected with a 90° geometry with a 4× microscopy objective. A long-pass edge filter at 550 nm (Thorlabs) was used to reject the scattered exciting radiation. A Czerny–Turner monochromator (Andor Shamrock 500i) equipped with a 300 lines mm^{-1} grating and with a Peltier-cooled (−80 °C) CCD camera (Andor, iDus) was used to collect the luminescence spectra. A slit width of 10 μm was used for the measurements. The excitation spectra were measured with a spectrofluorometer (Fluorolog, Horiba), using an optical resolution of 1 nm. The same experimental setup, in pulsed mode, was also used to measure the emission decays.

Acknowledgements

F.L.P. and G.M. thank the European Union (NextGeneration EU) for support within the SAMOTHRACE project (grant no. ECS00000022). A.L.P. thanks the Ministero dell'Università e della Ricerca within the PON FSE REACT-EU 2014–2020 Azioni IV.4. This work was also supported by the PRIN-PNRR project for Mission 4-Component 2-Investment 1.1, financed by European Union Next Generation EU, project no. P2022XMF43 "OPTIMISE", and the Italian Ministry of University and Research (MUR), Italy. The authors thank Bionanotech Research and Innovation Tower (BRIT) laboratory of University of Catania (grant no. PONa3_00136 financed by the Italian Ministry for Education, University and Research, MIUR) for the diffractometer facility.

Conflict of Interest

The authors declare no conflict of interest.

Author Contributions

Anna Lucia Pellegrino: conceptualization (lead); data curation (equal); methodology (lead); writing—original draft (lead). **Francesca Lo Presti**: data curation (equal); investigation (equal). **Francesca Loschi**: investigation (equal). **Adolfo Speghini**: methodology (equal); supervision (equal); writing—review & editing (supporting). **Graziella Malandrino**: funding acquisition (lead); supervision (lead); writing—review & editing (equal).

Data Availability Statement

The data that support the findings of this study are available from the corresponding author upon reasonable request.

Keywords

Eu-doping, hexagonal $NaGdF_4$, thin films, X-ray diffractions

Received: September 4, 2024
Revised: February 16, 2025
Published online:

[1] R. A. Janjua, W. Ji, N. A. Shah, J. Evans, R. Zhang, S. Zhang, S. He, *Prog. Electromagn. Res. M.* **2023**, *122*, 117.
[2] H. Xu, M. Dai, Z. Fu, *Small* **2024**, *20*, 2400218.
[3] C. Huang, P. Li, X. Li, J. Gu, N. Fu, W. Zhang, *Sol. RRL* **2023**, *7*, 2300518.
[4] Y. S. Liu, D. T. Tu, H. M. Zhu, X. Y. Chen, *Chem. Soc. Rev.* **2013**, *42*, 6924.
[5] N. C. Dyck, F. C. J. M. Van Veggel, G. P. Demopoulos, *ACS Appl. Mater. Interfaces* **2013**, *5*, 11661.
[6] G. L. Peña, E. O. Mansilla, A. Arranz, N. Bogdan, M. M. Silván, E. M. Rodríguez, *Colloids Surf. B: Biointerfaces* **2024**, *239*, 113934.
[7] G. López-Peña, A. R. García, J. G. Solé, E. M. Rodríguez, *J. Lumin.* **2024**, *274*, 120701.
[8] J. J. Velázquez, R. Balda, J. Fernández, G. Gorni, L. Pascual, G. Chen, M. Sundararajan, A. Durán, M. J. Pascual, *J. Lumin.* **2018**, *193*, 61.
[9] J. J. Velázquez, R. Balda, J. Fernández, G. Gorni, G. C. Mather, L. Pascual, A. Durán, M. J. Pascual, *J. Non-Cryst. Solids* **2018**, *501*, 136.
[10] F. L. Presti, A. L. Pellegrino, E. Milan, E. Radicchi, A. Speghini, G. Malandrino, *J. Mater. Chem. C* **2023**, *11*, 12195.
[11] B. Liu, H. Tan, Y. Chen, *Anal. Chim. Acta* **2013**, *761*, 178.
[12] S. Liu, Y. Li, C. Zhang, L. Yang, T. Zhao, R. Zhang, C. Jiang, *J. Colloid Interface Sci.* **2017**, *493*, 10.
[13] M. Alkahtani, A. A. Almuqhim, H. Qasem, N. Alsofyani, A. Alfahd, S. M. Alenzi, A. Aljuwayr, Y. A. Alzahrani, A. Al-Badri, M. H. Alotaibi, A. Bagabas, A. N. AlHazaa, P. R. Hemmer, *Sol. Cell.* **2021**, *11*, 2909.
[14] L. Francés-Soriano, J. Ferrera-González, M. González-Béjar, J. Pérez-Prieto, *Anal. Bioanal. Chem.* **2022**, *414*, 4291.
[15] J. Wu, S. Wei, X. Weng, R. Wang, H. Zhou, S. Cheng, *Sol. Energy Mater. Sol. Cells* **2022**, *248*, 112029.
[16] Pushpendra, R. K. Kunchala, S. N. Achary, B. S. Naidu, *ACS Appl. Nano Mater.* **2019**, *2*, 5527.
[17] Pushpendra, I. Suryawanshi, S. Srinidhi, S. Singh, R. Kali, R. K. Kunchala, S. L. Mudavath, B. S. Naidu, *Mater. Today Commun.* **2021**, *26*, 102144.
[18] H. Jia, Y. Zhou, X. Li, Y. Li, W. Zhang, H. Fu, J. Zhao, L. Pan, X. Liu, J. Qiu, *CrystEngComm* **2018**, *20*, 6919.
[19] F. Venne, M. Quintanilla, F. Quenneville, D. Işik, B. Baloukas, F. Vetrone, C. Santato, *RSC Adv.* **2015**, *5*, 81875.
[20] R. Chen, J. Xu, J. Xu, H. Lin, Y. Cheng, Y. Wang, *J. Lumin.* **2024**, *270*, 120575.
[21] V. V. Bakhmetyev, A. M. Dorokhina, M. V. Keskinova, S. V. Mjakin, A. B. Vlasenko, L. A. Lebedev, V. V. Malygin, M. M. Sychov, *Chem. Pap.* **2020**, *74*, 787.
[22] P. Ghosh, R. K. Sharma, Y. N. Chouryal, A. V. Mudring, *RSC Adv.* **2017**, *7*, 33467.
[23] M. E. Cruz, T. Ngoc Lam Tran, A. Chiasera, A. Durán, J. Fernandez, R. Balda, Y. Castro, *Nanomaterials* **2023**, *13*, 940.
[24] J. J. Velázquez, J. Mosa, G. Gorni, R. Balda, J. Fernández, A. Durán, Y. Castro, *J. Non-Cryst. Solids* **2019**, *520*,119447.
[25] M. Quintanilla, E. Hemmer, J. Marques-Hueso, S. Rohani, G. Lucchini, M. Wang, R. R. Zamani, V. Roddatis, A. Speghini, B. S. Richards, F. Vetrone, *Nanoscale* **2022**, *14*, 1492.
[26] A. L. Pellegrino, E. Milan, A. Speghini, G. Malandrino, *Materials* **2023**, *16*, 6889.
[27] A. L. Pellegrino, M. R. Catalano, P. Cortelletti, G. Lucchini, A. Speghini, G. Malandrino, *Photochem. Photobiol. Sci.* **2018**, *17*, 1239.
[28] M. R. Catalano, A. L. Pellegrino, P. Rossi, P. Paoli, P. Cortelletti, M. Pedroni, A. Speghini, M. Malandrino, *New J. Chem.* **2017**, *41*, 4771.
[29] R. D. Shannon, *Acta Crystallogr.* **1976**, *32*, 751.
[30] F. Lo Presti, A. L. Pellegrino, E. Milan, E. Radicchi, A. Speghini, G. Malandrino, *J. Mater. Chem. C* **2023**, *11*, 12195.
[31] B. Bondzior, P. J. Dereń, *J. Lumin.* **2018**, *201*, 298.
[32] A. M. Srivastava, M. G. Brik, W. W. Beers, W. Cohen, *Opt. Mater.* **2021**, *114*, 110931.
[33] P. Ptacek, H. Schäfer, K. Kömpe, M. Haase, *Adv. Funct. Mater.* **2007**, *17*, 3843.
[34] P. Ptacek, H. Schäfer, K. Kömpe, M. Haase, *Cryst. Growth Des.* **2010**, *10*, 589.

[35] P. Ghosh, S. Tang, A.-V. Mudring, *J. Mater. Chem.* **2011**, *21*, 8640.
[36] Y. Li, S. Natakorn, Y. Chen, M. Safar, M. Cunningham, J. Tian, D. D.-U. Li, *Front. Phys.* **2020**, *8*, 576862.
[37] P. V. Do, N. X. Ca, L. D. Thanh, D. D. Quan, N. M. Hung, P. T. Du, N. T. Huong, D. T. Anh, *Phys. Chem. Chem. Phys.* **2023**, *25*, 28296.
[38] G. Malandrino, O. Incontro, F. Castelli, I. L. Fragalà, C. Benelli, *Chem. Mater.* **1996**, *8*, 1292.
[39] G. Malandrino, M. Bettinelli, A. Speghini, I. Luciano Fragalà, *Eur. J. Inorg. Chem.* **2001**, *2001*, 1039.
[40] J. J. Burns. *Inorg. Chem.* **1965**, *4*, 882.